Research article

Journal of MASS SPECTROMETRY

Received: 11 February 2015 Revised: 8 May 2015 Accepted: 16 May 2015 Published online in Wiley Online Library

(wileyonlinelibrary.com) DOI 10.1002/jms.3617

Effects of GC temperature and carrier gas flow rate on on-line oxygen isotope measurement as studied by on-column CO injection

Zhi-Gang Chen,[a,b] Xi-Jie Yin[c]* and Youping Zhou[d,e]

Although deemed important to $\delta^{18}O$ measurement by on-line high-temperature conversion techniques, how the GC conditions affect $\delta^{18}O$ measurement is rarely examined adequately. We therefore directly injected different volumes of CO or CO–N_2 mix onto the GC column by a six-port valve and examined the CO yield, CO peak shape, CO–N_2 separation, and $\delta^{18}O$ value under different GC temperatures and carrier gas flow rates. The results show the CO peak area decreases when the carrier gas flow rate increases. The GC temperature has no effect on peak area. The peak width increases with the increase of CO injection volume but decreases with the increase of GC temperature and carrier gas flow rate. The peak intensity increases with the increase of GC temperature and CO injection volume but decreases with the increase of carrier gas flow rate. The peak separation time between N_2 and CO decreases with an increase of GC temperature and carrier gas flow rate. $\delta^{18}O$ value decreases with the increase of CO injection volume (when half *m/z* 28 intensity is <3 V) and GC temperature but is insensitive to carrier gas flow rate. On average, the $\delta^{18}O$ value of the injected CO is about 1‰ higher than that of identical reference CO. The $\delta^{18}O$ distribution pattern of the injected CO is probably a combined result of ion source nonlinearity and preferential loss of $C^{16}O$ or oxygen isotopic exchange between zeolite and CO. For practical application, a lower carrier gas flow rate is therefore recommended as it has the combined advantages of higher CO yield, better N_2–CO separation, lower He consumption, and insignificant effect on $\delta^{18}O$ value, while a higher-than-60 °C GC temperature and a larger-than-100 μl CO volume is also recommended. When no N_2 peak is expected, a higher GC temperature is recommended, and vice versa. Copyright © 2015 JohnWiley & Sons, Ltd.

Additional supporting information may be found in the online version of this article at the publisher's website.

Keywords: oxygen isotope; high-temperature conversion; on-line continuous flow; GC temperature; carrier gas flow rate; N_2–CO separation

Introduction

The large relative mass differences between their isotopes and thus wide natural range of their isotopic compositions (isotopic ratios) make the isotopes of light elements (e.g. C, H, O, N, and S) favorite natural tracers in a wide range of studies.[1–3] The isotopic composition of light elements is usually measured by isotope ratio mass spectrometer (IRMS), which requires converting the interested elements into a suitable analyte gases first. The technique of analyte gas preparation and introduction has evolved from offline conversion and dual-inlet introduction prior to the 1980s to now-popular on-line continuous flow (CF) introduction with carrier gas, which is accomplished by elemental analyzer (EA) for nitrogen,[4] carbon,[5] or sulfur,[6] and high-temperature conversion (HTC) for oxygen[7] or hydrogen[8] isotopes. Although the on-line CF technique has the combined advantages of easy operation, high throughput, minimal sample amount requirement, and suitability to multi-types of samples (especially for oxygen),[9,10] it does have the easily ignored on-line isotope fractionation and contamination issues. A lack of knowledge of such problems may compromise the quality of isotopic data.[11]

For oxygen isotope analysis by HTC, the oxygen in the sample is first pyrolytically converted to analyte gas CO in a high-temperature reactor and further separated from other gases such as N_2, CO_2, and H_2 on a GC column, usually a 5-Å molecular sieve (zeolite). After eluting from the GC column, the CO is transferred into an IRMS via an open-split interface for oxygen isotope ratio measurement. The conversion and separation processes are the most likely steps where isotopic fractionation can occur. Although there are many studies on the effects of conversion process on the oxygen isotope measurement,[9,12–15] there are very few studies on the effect of the separation process. Theoretically, the GC conditions can affect the CO yield, peak shape, gas separation, and even the isotope exchange between the adsorbent and adsorbate. Indeed, many studies have shown that GC can lead to carbon isotope fractionation[1,16,17] and GC conditions have significant influences on the $\delta^{13}C$[14,18,19] and $\delta^{15}N$ measurements.[20] For the commercially available 5-Å molecular sieve (zeolite)-based column whose physical properties are factory-set, GC temperature and carrier gas flow

* *Correspondence to: Xi-Jie Yin, The Third Institute of Oceanography, State Oceanic Administration, Xiamen 361005, China. E-mail: yinxijie2003@163.com*

a *College of Ocean and Earth Sciences, Xiamen University, Xiamen 361102, China*

b *Key Laboratory of Coastal and Wetland Ecosystems, Ministry of Education, Xiamen University, Xiamen 361102, China*

c *The Third Institute of Oceanography, State Oceanic Administration, Xiamen 361005, China*

d *Institute for Landscape Biogeochemistry, ZALF, Müncheberg, Germany*

e *Leibniz Institute of Freshwater Ecology and Inland Fisheries, Neuglobsow, Germany*

rate are the only two adjustable parameters. At present, the applied GC temperature varies from room temperature to 90 °C, and the carrier gas flow rate varies from 60 to 120 ml/min among different laboratories.[21–25] The lack of consensus about the optimal GC conditions and their effects on $\delta^{18}O$ measurements warrants further studies reported in this paper. We addressed this issue by injecting CO or CO–N_2 mix directly onto GC column (on-column injection) via a six-port valve on an HTC system we previously used.[12] This way, we effectively bypassed the HTC process, allowing us to gauge the effects of GC column conditions on oxygen isotopic measurements. We specifically investigated the effects of sample amount, GC temperature, and carrier gas flow rate on CO yield, CO peak shape, CO–N_2 separation, and $\delta^{18}O$ value.

Experimental

Material

The measurement system is the same one we used to measure HTC oxygen yields of organic and inorganic solids by on-column CO injection.[12] Briefly, it comprises a six-port injection valve, a TC/EA unit (HTC unit), a ConFlo III open-split interface, and an IRMS.

The HTC system used in this study is a Flash HT (1112 Series) – Delta V Advantage (Thermo Fisher) (Fig. 1(c, d, and e)). The working gas is high-purity CO (99.9999%) with $\delta^{18}O_{VSMOW} = 8.8‰$, which is calibrated by two international oxygen isotope reference materials, i.e. the IAEA-601 benzoic acid ($\delta^{18}O_{VSMOW} = 23.2‰$) and Ag_3PO_4 ($\delta^{18}O_{VSMOW} = 21.7‰$) (Elemental Microanalysis Ltd, Part No: B2207, Certificate No: BN180097). The carrier gas is He (99.9999%). The GC column used in this study is a stainless-steel tube (1.0 m, 10 mm o.d., SA990724, SANTIS) filled with 5-Å molecular sieve. The model of open-split is ConFlo III. The six-port valve is of the manual operation type of VICI (MNK250414), and the sizes of the sample loops are 50, 100, 250, and 500 μl, respectively.

Configuration of the measurement system

One port of the six-port valve is connected to the GC column directly (Fig. 1(a, b)). The six-port valve is also connected to the He carrier gas cylinder and CO working gas cylinder (or a CO–N_2 mix airbag for the 'second experiment' as described later in the text). A CO valve is placed between the CO working gas cylinder and the six-port valve (Fig. 1(a, b)). After the third reference peak is eluted (Fig. 1(e)), the CO valve is first opened to fill the sample loop with CO ('CO sampling', Fig. 1(a)); after that, the CO valve is closed, and the six-port valve is switched on immediately, allowing the carrier gas to flush the CO from the sample loop into the GC column ('CO injecting', Fig. 1(b)). Then the CO flows into the IRMS via the sample open-split interface (Fig. 1(c)). The sample open-split has two modes ('dilution on' and 'dilution off', which will be introduced in more detail in the later section). In this study, all the experiments were carried out under the 'dilution off' mode. The CO of the reference peak comes directly from the working gas cylinder and flows into the IRMS from the reference open-split (Fig. 1(c)). Throughout this paper, the CO that flows into the IRMS through the reference open-split and its peak or $\delta^{18}O$ value is referred to as 'reference CO' to differ from the on-column injected CO, which is referred to as 'injected CO'. The $\delta^{18}O$ value is processed by the software ISODAT 3.0. An empty airbag is connected to the CO vent of the six-port valve to collect the toxic surplus of CO.

Methods

We designed three experiments. The first experiment was designed to study the effects of sample amount, GC temperature, and carrier

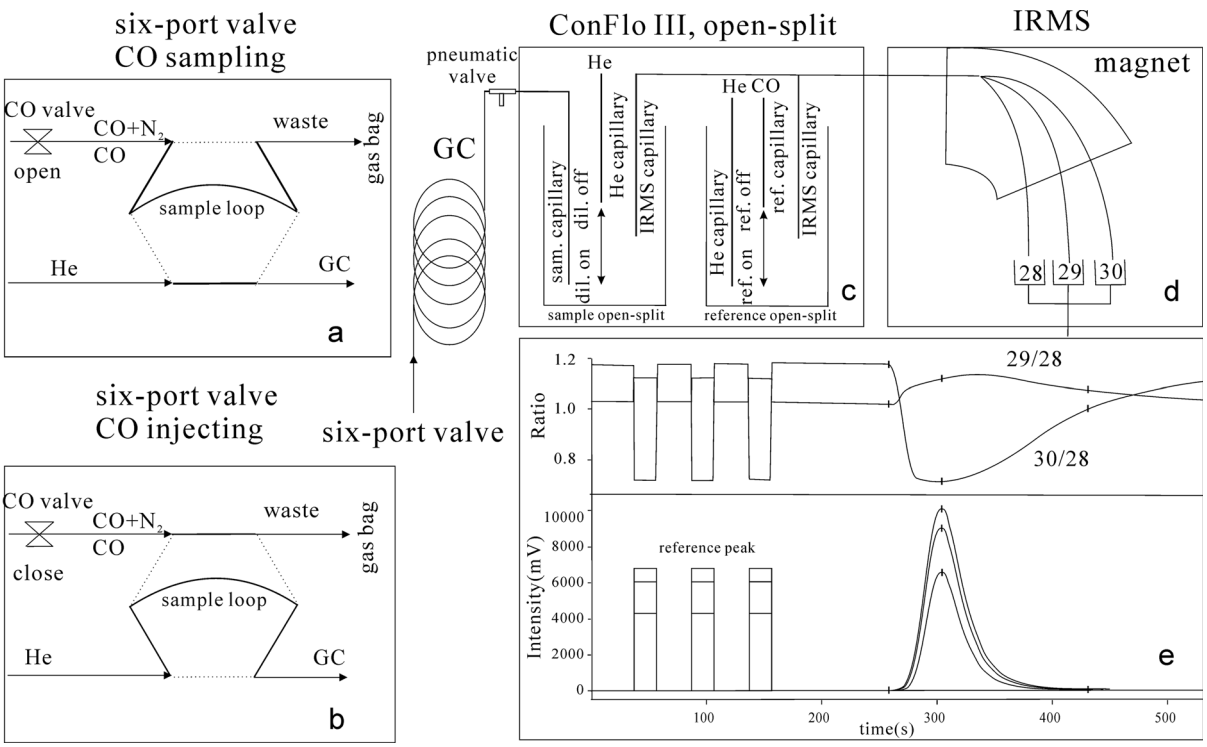

Figure 1. The configuration of the HTC system used in this study as modified from Yin and Chen.[12]

Journal of MASS SPECTROMETRY

gas flow rate on CO yield, peak shape, and $\delta^{18}O$ value; we varied the CO injection volume (50, 100, 250, and 500 μl), carrier gas flow rate (60, 77, and 100 ml/min), and GC temperature (60, 85 and 100 °C) and analyzed the CO yield, peak shape, and $\delta^{18}O$ value.

The second experiment was designed to study the effects of GC temperature and carrier gas flow rate on the separation of CO and N_2. Prior to injection, we mixed CO and N_2 in a ratio of 2 : 1 (v : v) in a clean and evacuated airbag and connected the airbag to one port of the six-port valve, which was connected to the CO valve and CO working gas cylinder in the 'first experiment'. Except the filling of the sample loop was accomplished by gently pressing the CO–N_2 mix airbag, the rest of the procedures are the same as the 'first experiment'. The experiment was conducted with one injection volume (50 μl), four different carrier gas flow rates (50, 60, 70, and 80 ml/min), and five different GC temperatures (30, 35, 43, 50, and 60 °C).

The third experiment was designed to study the effect of reference peak intensity on its $\delta^{18}O$ value. We took the advantage offered by the ISODAT 3.0 'Reference ON and OFF' method editor to measure the $\delta^{18}O$ value of reference peak repeatedly: When a reference peak is eluted, the pressure of the working gas is adjusted manually through the ConFlo III immediately while keeping the peak width stable (Fig. S2). This method is essentially the same as the 'linearity test' described in the instrument manual. The intensity of the reference peak used to calculate the $\delta^{18}O$ value of reference peaks was similar to the one used for the injected CO.

For all three experiments, following each instrumental restart, $\delta^{18}O$ value measurement was attempted only after the standard deviation of the repeated $\delta^{18}O$ measurement of reference peaks (with stable intensity) is better than 0.06‰.

Results and discussion

Effects of GC conditions on the CO yield

High oxygen yield is important for precise isotopic measurement, and it is controlled by the HTC process and post-HTC process. Until now, most of the related studies are mainly focused on the former.[12] We therefore injected different volumes of CO onto the GC column and studied the CO yield of the post-HTC process under different GC temperatures and carrier gas flow rates (the 'first experiment'). Because the CO gas in the open-split is open to ambient air (discussed in the succeeding text) (Fig. 1(c)) and the efficiency of ionization and detection is unknown, it is difficult to determine the absolute CO yield; thus, we used the CO peak area as a substitute of CO yield as it is proportional to the latter.

Figure 2 shows the relationship between the CO peak area and carrier gas flow rate. It is clear that the CO peak area decreases linearly with carrier gas flow rate; the larger the CO injection volume is, the larger the decrease rate is. By extrapolating, we can see when the carrier gas flow rate approaches 160 ml/min, the CO peak area approaches zero for all CO injection volumes. Figure 2 also shows that the GC temperature has little effect on the CO peak area. We believe it is the ConFlo III open-slit that causes the observed decrease of CO peak area with an increasing carrier gas flow rate. The ConFlo III has two open-splits, one for sample gas and the other for reference gas. The sample open-split is made up of a cell and three capillaries (Fig. 1 (c)).[26] The capillary on the right is the IRMS capillary, which delivers the sample gas into the IRMS. The one in the middle is the He capillary, which can move up and down under the control of the ISODAT 3.0 software. When the He capillary moves down, the open-split is in the 'dilution on' mode; that is, the He from the He capillary can blow most of the sample gas out of the cell, and only a small portion of the sample gas can flow into the IRMS. When the He capillary moves up, the open-split is in the 'dilution off' mode; that is, the He from the He capillary can form a He atmosphere at the top of the cell to protect the sample gas, and a larger portion of sample gas can flow into the IRMS. The sample gas that elutes from the GC column flows into the sample open-split through the sample capillary, which is positioned on the left side and deeper than the IRMS capillary. The reference open-split, which directly delivers the working gas into the IRMS, is similar to the sample open-split. The only difference between the two (open-slits) is in the capillary that moves: In the case of the sample open-split, the moving capillary is the He capillary, while in the reference open-split, it is the CO capillary (Fig. 1 (c)).

After leaving the GC column, the gases first pass a pneumatic valve (Fig. 1 (c)), which diverts most of the gases at a stable ratio (81/81.5 when 'dilution on', 73.5/81.5 when 'dilution off').[26] Because the flow rate of the IRMS capillary (~0.3 ml/min) is stable and lower than that of sample capillary,[26] even in the 'dilution off' mode, a portion of sample gas will flow out of the cell and will be lost to the ambient air. Therefore, when the carrier gas (sample capillary) flow rate increases, more sample gas will be blown out of the cell, leading to a decrease of the CO peak area. As larger CO injection volume will have a higher CO concentration, longer residence time in the cell, and proportionally more CO being blown out, a larger decrease rate in CO peak area will be expected.

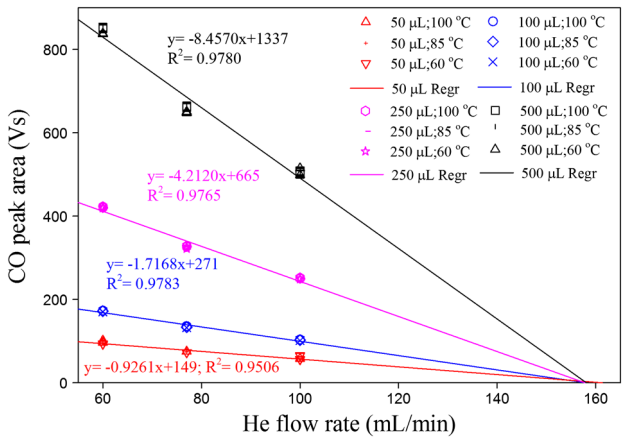

Figure 2. The relationship between CO peak area and He flow rate.

Effects of GC condition on the CO peak shape

Although peak shape is very important for the precise isotopic composition measurement and is knowingly affected by the GC conditions,[20] relevant study (in particular 5-Å molecular sieve-based GC) is surprisingly rare. We investigated the effect of GC column temperature and carrier gas flow rate on the two indicators of peak shape, i.e. CO peak width and intensity, by injecting different volumes of CO onto the GC column (the 'first experiment'). The results are presented in Figs 3 and 4.

For the effects of GC temperature, the results show that the CO peak (*m/z* 28) width decreases with the increase of GC temperature but the rate of decrease is insensitive to both the carrier gas flow rate and CO injection volume (Fig. 3). The CO peak intensity increases with the increase of GC temperature, and the rate of increase is higher when CO injection volume is larger (Fig. 4). For the effects of GC temperature on peak width, Jennings remarked

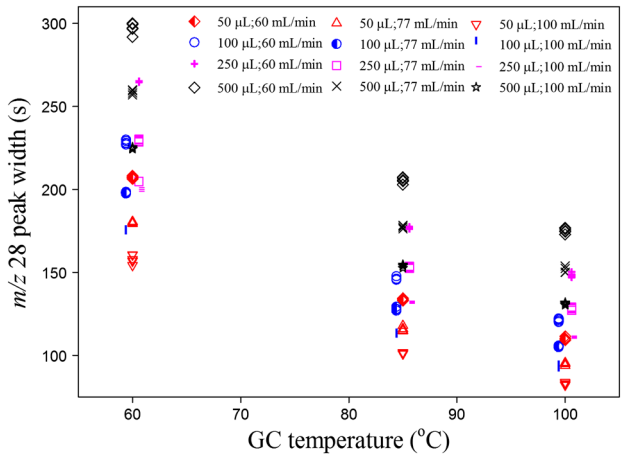

Figure 3. The relationship between the *m/z* 28 peak width and the three GC temperatures (60, 85, and 100 °C) tested in this study.

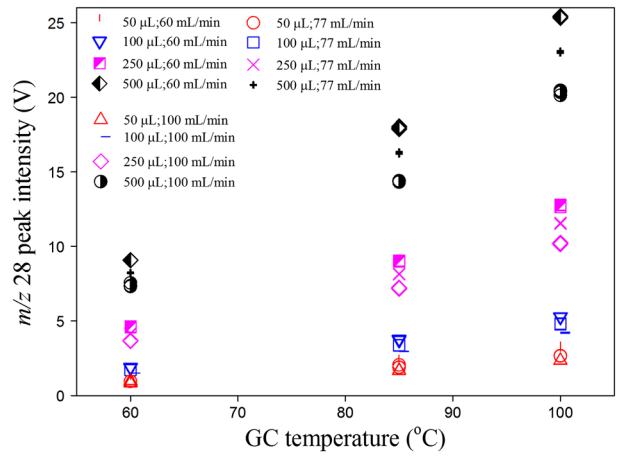

Figure 4. The relationship between the *m/z* 28 peak intensity and the three GC temperatures (60, 85, and 100 °C) tested in this study.

'Consideration of van Deemter equation makes it apparent that temperature effects will be interrelated and that the precise overall result of a temperature change is not easily defined'.[27] On the contrary, our results clearly show that under the conditions used in this study (He as the carrier gas and 5-Å molecular sieve as stationary phase), an increase of GC temperature leads to a decrease of CO peak width. Similar decrease rate (Fig. 3) indicates that the effect of temperature on the CO peak width does not depend on the CO injection volume and carrier gas flow rate. For a given carrier gas flow rate and CO injection volume, the CO peak areas are stable for different GC temperatures (Fig. 2). Because peak area is roughly the product of peak width and peak intensity, a decrease in peak width should lead to a corresponding increase in peak intensity. This is confirmed in Fig. 4.

For the effects of carrier gas flow rate, Figs 3 and 4 show that at a given GC temperature and CO injection volume, both CO peak width and intensity decrease with the increase of carrier gas flow rate. This is against the prediction that peak width and intensity should show opposite relationships with carrier gas flow rate under the assumption that there is no CO loss. At the same time, the van Deemter equation shows that the peak width at first decreases with the increase of carrier gas flow rate (controlled by molecular diffusion process); however, after peak width reaches the narrowest point, it begins to increase with the increase of carrier gas flow rate (controlled by mass transfer processes).[27] We believe these discrepancies are the result of CO loss occurring in the open-split (as discussed in the preceding text): Higher CO loss at higher carrier gas flow rate overran the effect of carrier gas flow rate on the molecular diffusion process and mass transfer process.

The peak intensity/width ratio can be used to describe the peak shape. A higher intensity/width ratio means a sharper peak and a more precise δ value.[20] Figure S1 shows the relationship between the GC temperature and the CO peak intensity/width ratio. It is clear that the ratio increases with the increase of the GC temperature, with a higher increase rate at larger CO injection volume, while the carrier gas flow rate has little influence on it. So, although both the GC temperature and carrier gas flow rate can influence the CO peak width and intensity, the intensity/width ratio is mainly controlled by the GC temperature.

Effects of GC condition on CO–N_2 separation

N_2 is known to have significant interference on the $\delta^{18}O$ measurement because of the isobaric effect of NO^+ ($^{14}N^{16}O^+$) it may form (with O) in the ion source, which can lead to an erroneous higher signal for $^{12}C^{18}O^+$ (*m/z* 30).[28,29] Many methods have been used to circumvent such an issue, such as diverting the N_2 peak to waste by a four-port valve,[23,24,28,30,31] diluting N_2 via the 'He dilution' technique of the ConFlo open-split,[24,29,31] trapping the CO with a 5-Å molecular sieve column,[32,33] and inserting a CO reference peak between the peaks of N_2 and CO.[29] However, these methods are catered for samples that have high nitrogen content and require large N_2–CO peak separation time. For samples with no or low nitrogen content, the N_2-associated $^{14}N^{16}O^+$ isobaric effect can be resolved simply by enlarging N_2–CO peak separation time, which in turn can be accomplished chromatographically only by optimizing the GC conditions. Unfortunately, relevant study on the separation conditions of CO and N_2 by a 5-Å molecular sieve column is scarce.[24,34] We therefore conducted the second experiment by injecting N_2–CO mix onto the GC column and studied the peak separation time between N_2 and CO (the time difference between the end of N_2 peak and the start of CO peak) under different GC temperature and carrier gas flow rate conditions. The results are shown in Fig. 5.

It is clear that with the increase of the GC temperature and carrier gas flow rate, the peak separation time decreases steadily. Because

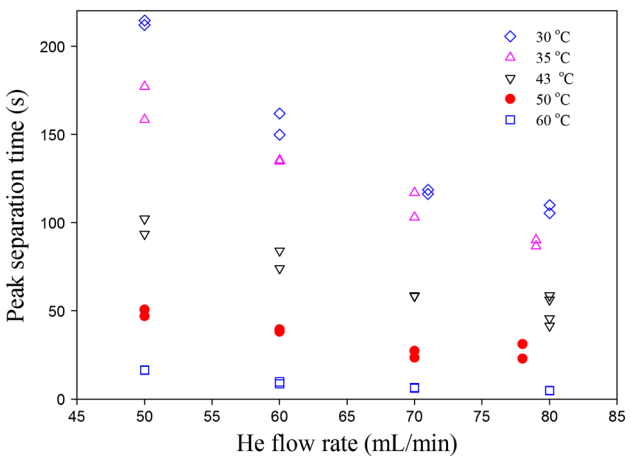

Figure 5. The relationship between CO–N_2 peak separation time and He flow rate.

Journal of MASS SPECTROMETRY

both carrier gas flow rate and GC temperature are inversely correlated with the retention time of the gas in the GC column,[35] an increase in GC temperature or carrier gas flow rate will lead to a larger decrease in retention time for the longer retention time peaks (than the shorter retention time peaks), therefore reducing the retention difference (separation time) between peaks. Although peak width decreases with increasing GC temperature and carrier gas flow rate (Fig. 3), which may lead to an increase in the separation time between two peaks, the unequal decrease in retention times between the two peaks offsets such (separation time) increase and leads to a final shortening of the separation time between the two peaks.

Our results are consistent with the findings that separation of CO and N_2 at 70 °C and 0.85 bar (carrier gas pressure, which is proportional to carrier gas flow rate) is better than that at 90 °C and 1.0 bar.[34] Accoe *et al.* also found that the GC temperature of 20 °C is the optimal setting for N_2–CO separation, but their optimal He flow rate is a little bit higher (90 ml/min).[24] Thus, it can be concluded that a higher GC temperature produces a better peak shape but worse N_2–CO separation (and vice versa), while a lower carrier gas flow rate gives acceptable peak shape and better separation.

One should note that the HTC by-products of the nitrogen-bearing material also include other gases such as hydrogen cyanide or cyanogen. As these by-products can degrade the GC column performance and affect ionization efficiency as they enter the IRMS ion source,[15,31] so it is better to remove them (by trapping or diverting) before the GC column. However, this is beyond the scope of the current study.

Effect of sample amount on the $\delta^{18}O$ value

Some studies found $\delta^{18}O$ value to vary with sample amount,[19,36–40] a phenomenon usually referred as ion source nonlinearity. Most studies show a positive relationship between $\delta^{18}O$ value and sample amount,[19,38–40] while others show a negative relationship,[36] and a few more show both positive and negative relationships.[37] In this paper, we give a detailed study about the relationship between $\delta^{18}O$ value and sample amount (the 'first experiment'). The results are shown in Fig. 6.

The upper part of Fig. 6 shows the result of the injected CO. Note that we used the half *m/z* 28 peak intensity to approximate its mean intensity. For comparison, the effects of reference intensity to the $\delta^{18}O$ value of reference peak were also studied (the 'third experiment'). The results are shown in the lower part (represented by the empty stars) of Fig. 6 (see also Figure S2 for the mass chromatogram). It is clear when the half *m/z* 28 peak intensity is low (<3 V), the $\delta^{18}O$ values of both injected CO and reference CO decrease with the increase of intensity (Fig. 6). However, when the half *m/z* 28 peak intensity is above 3 V, the $\delta^{18}O$ values tend to be stable. Because the reference CO comes directly from the CO working gas cylinder (Fig. 1(c)) and the GC conditions were kept unchanged during the $\delta^{18}O$ measurement of reference CO, the inverse relationship between $\delta^{18}O$ value and peak intensity of the reference CO should be the result of ion source nonlinearity. Similarly, the inverse relationship for the injected CO should be at least partially caused by the same ion source nonlinearity too. Because the nonlinearity is nearly absent when the half *m/z* 28 peak intensity is above 3 V, so this value is recommended for better $\delta^{18}O$ measurement precision. It is also clear that the $\delta^{18}O$ value of injected CO is about 1‰ higher than that of reference CO. We will discuss the cause of such discrepancy in the last section.

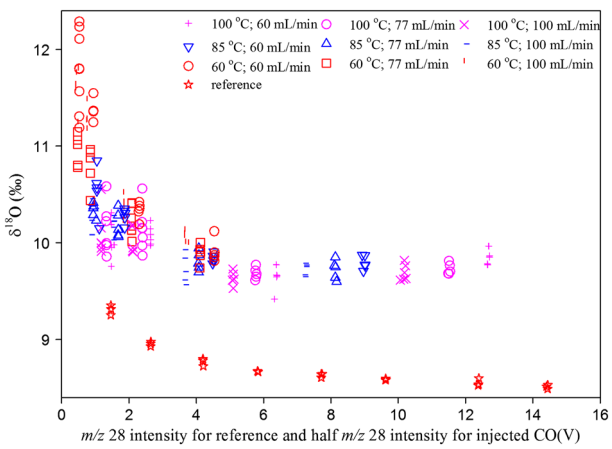

Figure 6. The relationship between the $\delta^{18}O$ value and *m/z* 28 peak intensity (for the reference CO) or half *m/z* 28 peak intensity (for the injected CO). The stars at the lower part of the figure represent the reference CO; all the other symbols represent the injected CO.

Effect of carrier gas flow rate on the $\delta^{18}O$ value

Figure 7 shows the relationship between the $\delta^{18}O$ value and carrier gas flow rate. Except for the analyses conducted with 50 and 100 μl injection volumes at GC temperature of 60 °C, the $\delta^{18}O$ value does not vary with the carrier gas flow rate. Because the CO peak intensity decreases with the increase of carrier gas flow rate (Fig. 4), and the $\delta^{18}O$ value increases with the decrease of CO peak intensity (when half *m/z* 28 intensity is <3 V, ion source nonlinearity) (Fig. 6), so if the $\delta^{18}O$ value was controlled only by the intensity, at certain GC temperature and CO injection volume (especially when half *m/z* 28 intensity is <3 V), the $\delta^{18}O$ value should increase with the increase of carrier gas flow rate. But Fig. 7 shows $\delta^{18}O$ value nearly has no relationship with carrier gas flow rate, implying that other factor(s) must act to decrease the $\delta^{18}O$ value of the injected CO with the increase of carrier gas flow rate. As will be discussed in the last section, higher carrier gas flow rate can lead to weaker interaction (oxygen exchange and preferential $C^{16}O$ retention) between CO and 5-Å molecular sieve, which may be the candidate cause. To our best knowledge, there is only one similar study that showed both $\delta^{18}O$ and $\delta^{13}C$ values of the injected CO increase with the increase of carrier gas pressure (flow rate).[14] The authors attributed the apparently opposite isotope–flow rate relationship to 'the

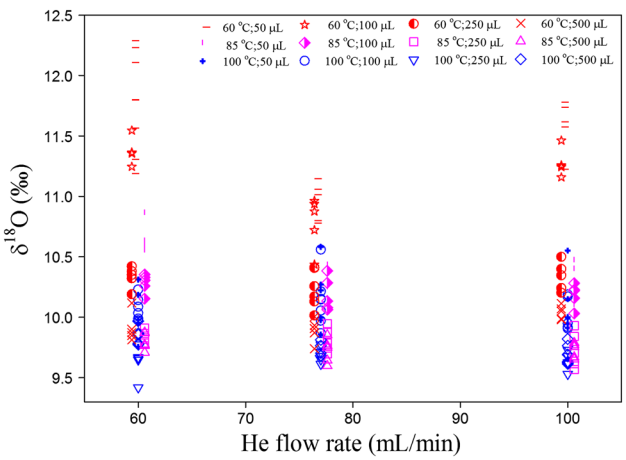

Figure 7. The relationship between the $\delta^{18}O$ value and the three carrier gas flow rate (60, 77, and 100 ml/min) tested in this study.

carrier gas pressure dependent fractionation effect in the open-split of the ConFlo II device'. Because the only difference between our study and theirs is the model of ConFlo (III *vs* II), the only explanation for such isotopic difference is that ConFlo II device has intrinsically larger fractionation.

Based on the result of this study, the $\delta^{18}O$ value varies more when the GC temperature is lower than 60 °C and CO injections volume is smaller than 100 μl; for better precision of $\delta^{18}O$ measurement, a higher-than-60 °C GC temperature and larger-than-100 μl injection volume (4.5 μmol oxygen atoms) are recommended.

Effect of GC temperature on the $\delta^{18}O$ value

The relationship between the $\delta^{18}O$ value and GC temperature is shown in Fig. 8. It can be seen that (1) the $\delta^{18}O$ value decreases with the increase of GC temperature and (2) for the larger injection volumes and higher GC temperatures, the effect of the GC temperature is weaker. Because the CO peak intensity increases with the increase of the GC temperature (Fig. 4), and the $\delta^{18}O$ value decreases with the increase of CO peak intensity (when half *m/z* 28 intensity is <3 V, ion source nonlinearity) (Fig. 6), the observed decrease in $\delta^{18}O$ value with the increase of GC temperature is probably the indirect consequence of ion source nonlinearity. Elsig and Leuenberger[19] presented results showing that $\delta^{13}C$ value of CO_2 increases with the increase of GC temperature while the $\delta^{18}O$ value is independent of the GC temperature. The discrepancy between the two studies is probably due to the differences in analyte gases (CO *vs* CO_2) and/or GC column chemistries (unfortunately, no such GC column chemistry information is available in the Elsig and Leuenberger[19] paper).

Oxygen isotope fractionation of the injected CO

Figure 6 shows that the $\delta^{18}O$ value of the injected CO is about 1‰ higher than that of the reference CO. Because the injected CO and reference CO are from the same gas cylinder and if no oxygen isotope fractionation occurred to the injected CO, identical $\delta^{18}O$ values for the injected and reference CO should be expected. Four possible causes of the discrepancy are discussed in the following:

(1) Peak shape difference between the reference and injected CO. The peak shape of reference CO is rectangle, while that of the injected CO is Gaussian distribution with small tailing (Fig. 1(e)). Although the individual mass traces end at 500 s for the injected CO as shown in (Fig. 1(e)), the mass ratio (e.g. 30/28) trace extends beyond 500 s, implying that the ratio still has not returned to the baseline value. Consequently, ignoring the CO at the peak tail can lead to an error in the $\delta^{18}O$ value of injected CO. To gain better insights, we recalculated the $\delta^{18}O$ value of a CO peak by choosing different peak end times. Figure S3 shows that $\delta^{18}O$ value increases with the increase of peak end time, and when the peak end time is longer than 540 s, the $\delta^{18}O$ value tends to be stable. This indicates ignoring the CO at the peak tail can decrease the $\delta^{18}O$ value. Therefore, ignoring the CO at the peak tail should not be the cause. On the other hand, as $C^{16}O$ elutes ahead of $C^{18}O$ (Fig. S3), the chance for $C^{16}O$ loss due to processes such as adsorption onto the flow path inner surface and filling the empty sample open-split is higher than that for $C^{18}O$, which can increase the $\delta^{18}O$ value of the injected CO.

(2) Oxygen isotopic exchange between the 5 Å molecular sieve (zeolite) and CO. Although oxygen isotopes can exchange between zeolite and water, CO_2 or O_2 at certain conditions, and the extent of such exchange varies with adsorbate type, temperature, and the oxygen position, cation type, and grain size of zeolite,[41–43] no study on the possible oxygen isotopic exchange between CO and zeolite has been reported. If such exchange is indeed the cause of the $\delta^{18}O$ enrichment of the injected CO (about 1‰ higher than that of the reference CO), it must imply that the exchange can lead to a $\delta^{18}O$ value increase for the injected CO; that is, zeolite is more enriched in ^{18}O than CO. For the effects of carrier gas flow rate, as higher carrier gas flow rates means shorter CO residence time in the column and therefore less opportunity of oxygen isotopic exchange between CO and zeolite, so the $\delta^{18}O$ value of injected CO would be higher at lower flow rate. However, as discussed in the preceding text, lower carrier gas flow rate is also associated with higher CO peak intensity, which in turn is associated with a decrease of $\delta^{18}O$ value. Thus, the net effect of the carrier gas flow rate can still be the $\delta^{18}O$ value being stable with carrier gas flow rate (Fig. 7). For the effects of GC temperature, higher temperature should theoretically increase the extent of exchange, leading to an increase in $\delta^{18}O$ value. However, higher temperature is also associated with higher peak intensity, which in turn is associated with a drop in $\delta^{18}O$ value. But if the effect of GC temperature on peak intensity overwhelms its effect on isotopic exchange, the net effect of GC temperature can still lead to a decrease in the $\delta^{18}O$ value of the injected CO with the increase of GC temperature (Fig. 8). Clearly, the oxygen isotopic exchange mechanism is noncommittal at this stage. Further study is needed to address this issue.

(3) Preferential retaining of $C^{16}O$ by 5-Å molecular sieve. CO can be adsorbed completely by the 5-Å molecular sieve at 40 °C or ambient temperature[32] and can be desorbed completely at 105[32] or 150 °C.[33] Because our GC temperature sat between the adsorption and desorption temperatures of these studies, if some $C^{16}O$ is preferentially retained on the 5-Å molecular sieve, a corresponding enrichment of ^{18}O in the residual CO should occur. However, as the abundance of $C^{16}O$ is much higher than that of $C^{18}O$, a significant amount of $C^{16}O$ retention on the 5-Å molecular sieve is needed to have a significant $\delta^{18}O$ increase of the residual CO, and the amount of retained $C^{16}O$ should be inversely related to GC temperature. This is inconsistent with the results that (1)

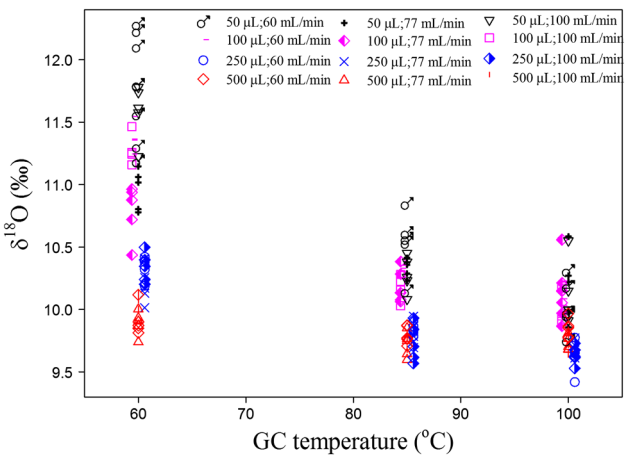

Figure 8. The relationship between the $\delta^{18}O$ value and the three GC temperatures (60, 85, and 100 °C) tested in this study.

Journal of MASS SPECTROMETRY

the yield of CO (mainly in the form of $C^{16}O$) has no clear relationship with the GC temperature (Fig. 2) and (2) $C^{18}O$ is preferentially retained by the 5-Å molecular sieve as implied by the fact that the $C^{18}O$ is enriched in the tail of the peak (see (1) of this section and Fig. S3). Further, there is evidence that ^{18}O, rather than ^{16}O, is preferentially retained on the 5-Å molecular sieve when O_2 is considered.[44,45] To conclude, the $C^{16}O$ preferential retained mechanism seems unlikely.

(4) Isotope fractionation in the open-split. Elsig and Leuenberger[19] found the $\delta^{13}C$ and $\delta^{18}O$ values of CO_2 that passes through the sample open-split are about 1‰ and 2.85‰, respectively, lower than that of the same CO_2 that passes through the reference open-split. They postulated that the CO_2 of the reference open-split has longer residence time and stronger diffusion than that of sample open-split, which leads to the CO_2 of the reference open-split being isotopically heavier than that of the sample open-split. If this is true, the isotope fractionation in the open-split clearly cannot be the cause, as it can lead to $\delta^{18}O$ value of the injected CO being lower than that of the reference CO.

Although we provide four mechanisms to explain the isotope fractionation of the injected CO, only the preferential loss of $C^{16}O$ or oxygen isotopic exchange (between 5-Å molecular sieve and CO) has the potential to cause the $\delta^{18}O$ value of the injected CO to be 1‰ higher than that of the reference CO. The exact cause still needs further study.

On the one hand, our study shows the $\delta^{18}O$ value of the injected CO is affected by the sample amount and GC temperature and is on average 1‰ higher than that of the identical reference CO. Therefore, if possible, the identical treatment principle as proposed by Werner[11] should be applied to obtain precise $\delta^{18}O$ value. On the other hand, this study also shows $\delta^{18}O$ value has a good exponential relationship with the intensity/width ratio of the CO peak (Fig. S4), which can be used to make correction for the $\delta^{18}O$ data when the sample matrix is identical or similar but other conditions such as sample amount, GC temperature, or carrier gas flow rate are varied.

Conclusions

In this work, we investigated the effects of GC temperature and carrier gas flow rate on N_2–CO separation, CO peak shape and yield, and $\delta^{18}O$ by injecting different volumes of CO or N_2–CO mix directly onto the GC column of an HTC system. Based on the results and discussions presented in the preceding text, we arrive at the following conclusions:

(1) The peak separation time between N_2 and CO decreases with the increase of GC temperature and carrier gas flow rate.

(2) The CO peak width increases with the increase of CO injection volume but decreases with the increase of GC temperature and carrier gas flow rate. CO peak intensity increases with the increase of GC temperature and CO injection volume but decreases with the increase of carrier gas flow rate. CO peak area decreases with the increase of carrier gas flow rate, and with a higher decrease rate for the larger CO volumes. GC temperature has little effect on the peak area.

(3) The $\delta^{18}O$ value of injected CO decreases with the increase of GC temperature and sample amount (when half *m/z* 28 intensity is <3 V) but is insensitive to carrier gas flow rate. On average, it is about 1‰ heavier than that of reference CO. The $\delta^{18}O$ distribution pattern of the injected CO probably is a combined result of ion source nonlinearity and preferential loss of $C^{16}O$ or oxygen isotopic exchange between zeolite and CO.

(4) For practical application, a lower carrier gas flow rate is recommended, for it has the combined advantage of larger CO yield, larger N_2–CO peak separation time, lower He consumption rate, and minimal effect on $\delta^{18}O$ value. A higher-than-60 °C GC temperature and a larger-than-100μl CO volume (4.5 μmol oxygen atoms) are also recommended. When no N_2 peak is expected, a higher GC temperature is recommended, and vice versa.

Acknowledgements

This study was supported by the NSFC (grant nos. 41006072, 41276059, and 40706033), Joint Foundation of NSFC-Yunnan (grant no. U1402232), and the Scientific Research Foundation of the Third Institute of Oceanography (grant no. 2013019). We appreciate the constructive comments of the two reviewers and Prof. Xi-Guang Zhang. Thanks to Ms. Cuicui Liang for the assistance with the isotopic measurement.

References

[1] W. Meier-Augenstein. Applied gas chromatography coupled to isotope ratio mass spectrometry. *J. Chromatogr. A* **1999**, *842*, 351.
[2] R. A. Werner. The online $^{18}O/^{16}O$ analysis: development and application. *Isot. Environ. Health Stud.* **2003**, *39*, 85–104.
[3] Y. P. Zhou, H. Stuart-Williams, G. D. Farquhar, C. H. Hocart. The use of natural abundance stable isotopic ratios to indicate the presence of oxygen-containing chemical linkages between cellulose and lignin in plant cell walls. *Phytochemistry* **2010**, *71*, 982.
[4] T. Preston, N. J. P. Owens. Interfacing an automatic elemental analyser with an isotope ratio mass spectrometer: the potential for fully automated total nitrogen and nitrogen-15 analysis. *Analyst* **1983**, *108*, 971.
[5] T. Preston, N. J. P. Owens. Preliminary ^{13}C measurements using a gas chromatograph interfaced to an isotope ratio mass spectrometer. *Biom. Mass Spectrom.* **1985**, *12*, 510.
[6] F. Pichlmayer, K. Blochberger. Isotopic abundance analysis of carbon, nitrogen and sulfur with a combined elemental analyzer-mass spectrometer system. *Fresenius Z. Anal. Chem.* **1988**, *331*, 196.
[7] W. A. Brand, A. R. Tegtmeyer, A. Hilkert. Compound-specific isotope analysis: extending toward $^{15}N/^{14}N$ and $^{18}O/^{16}O$. *Org. Geochem.* **1994**, *21*, 585.
[8] H. J. Tobias, K. J. Goodman, C. E. Blacken, J. T. Brenna. High-precision D/H measurement from hydrogen gas and water by continuous-flow isotope ratio mass spectrometry. *Anal. Chem.* **1995**, *67*, 2486.
[9] B. E. Kornexl, R. A. Werner, M. Gehre. Standardization for oxygen isotope ratio measurement - still an unsolved problem. *Rapid Commun. Mass Spectrom.* **1999**, *13*, 1248.
[10] B. E. Kornexl, M. Gehre, R. Höfling, R. A. Werner. On-line $\delta^{18}O$ measurement of organic and inorganic substances. *Rapid Commun. Mass Spectrom.* **1999**, *13*, 1685.
[11] R. A. Werner, W. A. Brand. Referencing strategies and techniques in stable isotope ratio analysis. *Rapid Commun. Mass Spectrom.* **2001**, *15*, 501.
[12] X. J. Yin, Z. G. Chen. Measuring oxygen yields of a thermal conversion/elemental analyzer-isotope ratio mass spectrometer for organic and inorganic materials through injection of CO. *J. Mass Spectrom.* **2014**, *49*, 1298.
[13] J. Koziet. Isotope ratio mass spectrometric method for the on-line determination of oxygen-18 in organic matter. *J. Mass Spectrom.* **1997**, *32*, 103.
[14] M. C. Leuenberger, M. S. Filot. Temperature dependencies of high-temperature reduction on conversion products and their isotopic signatures. *Rapid Commun. Mass Spectrom.* **2007**, *21*, 1587.

[15] G. B. Hunsinger, C. A. Tipple, L. A. Stern. Gaseous byproducts from high-temperature thermal conversion elemental analysis of nitrogen- and sulfur-bearing compounds with considerations for δ^2H and δ^{18}O analyses. *Rapid Commun. Mass Spectrom.* **2013**, *27*, 1649.
[16] M. P. Ricci, D. A. Merritt, K. . H. Freeman, J. M. Hayes. Acquisition and processing of data for isotope-ratio-monitoring mass spectrometry. *Org. Geochem.* **1994**, *21*, 561.
[17] Z. Zencak, C. M. Reddy, E. L. Teuten, L. Xu, A. P. McNichol, O. Gustafsson. Evaluation of gas chromatographic isotope fractionation and process contamination by carbon in compound-specific radiocarbon analysis. *Anal. Chem.* **2007**, *79*, 2042.
[18] W. Meier-Augenstein, P. W. Watt, C. D. Langhans. Influence of gas chromatographic parameters on measurement of ^{13}C/^{12}C isotope ratios by gas-liquid chromatography-combustion isotope ratio mass spectrometry. *I. J. Chromatogr. A.* **1996**, *752*, 233.
[19] J. Elsig, M. C. Leuenberger. ^{13}C and ^{18}O fractionation effects on open-splits and on the ion source in continuous flow isotope ratio mass spectrometry. *Rapid Commun. Mass Spectrom.* **2010**, *24*, 1419.
[20] E. Bahlmann, S. M. Bernasconi, S. Bouillon, M. Houtekamer, M. Korntheuer, F. Langenberg, C. Mayr, M. Metzke, J. J. Middelburg, B. Nagel, U. Struck, M. Voß, K. C. Emeis. Performance evaluation of nitrogen isotope ratio determination in marine and lacustrine sediments: an inter-laboratory comparison. *Org. Geochem.* **2010**, *41*, 3.
[21] R. A. Werner, B. E. Kornexl, A. Roβmann, H. L. Schmidt. On-line determination of δ^{18}O values of organic substances. *Anal. Chim. Acta* **1996**, *319*, 159.
[22] G. D. Farquhar, B. K. Henry, J. M. Styles. A rapid on-line technique for determination of oxygen isotope composition of nitrogen-containing organic matter and water. *Rapid Commun. Mass Spectrom.* **1997**, *11*, 1554.
[23] J. K. Böhlke, S. J. Mroczkowski, T. B. Coplen. Oxygen isotopes in nitrate: new reference materials for ^{18}O:^{17}O:^{16}O measurements and observations on nitrate-water equilibration. *Rapid Commun. Mass Spectrom.* **2003**, *17*, 1835.
[24] F. Accoe, M. Berglund, B. Geypens, P. Taylor. Methods to reduce interference effects in thermal conversion elemental analyzer/continuous flow isotope ratio mass spectrometry δ^{18}O measurements for nitrogen-containing compounds. *Rapid Commun. Mass Spectrom.* **2008**, *22*, 2280.
[25] V. Grimes, M. Pellegrini. A comparison of pretreatment methods for the analysis of phosphate oxygen isotope ratios in bioapatite. *Rapid Commun. Mass Spectrom.* **2012**, *27*, 375.
[26] R. A. Werner, B. A. Bruch, W. A. Brand. ConFlo III – an interface for high precision δ^{13}C and δ^{15}N analysis with an extended dynamic range. *Rapid Commun. Mass Spectrom.* **1999**, *13*, 1237.
[27] W. Jennings. *Analytical Gas Chromatography*. Academic Press Inc.: Orlando, Florida, **1987**.
[28] W. A. Brand, T. B. Coplen, A. T. Aerts-Bijma, J. K. Böhlke, M. Gehre, H. Geilmann, M. Gröning, H. G. Jansen, H. A. J. Meijer, S. J. Mroczkowski, H. Qi, K. Soergel, H. Stuart-Williams, S. M. Weise, R. A. Werner . Comprehensive inter-laboratory calibration of reference materials for δ^{18}O versus VSMOW using various on-line high-temperature conversion techniques. *Rapid Commun. Mass Spectrom.* **2009**, *23*, 999.
[29] M. Gehre, G. Strauch. High-temperature elemental analysis and pyrolysis techniques for stable isotope analysis. *Rapid Commun. Mass Spectrom.* **2003**, *17*, 1497.
[30] H. P. Qi, T. B. Coplen, L. I. Wassenaar. Improved online δ^{18}O measurements of nitrogen- and sulphur-bearing organic materials and a proposed analytical protocol. *Rapid Commun. Mass Spectrom.* **2011**, *25*, 2049.
[31] G. B. Hunsinger, L. A. Stern. Improved accuracy in high-temperature conversion elemental analyzer δ^{18}O measurements of nitrogen-rich organics. *Rapid Commun. Mass Spectrom.* **2012**, *26*, 554.
[32] H. P. Sieper, H. J. Kupka, L. Lange, A. Roßmann, N. Tanz, H. L. Schmidt. Essential methodological improvements in the oxygen isotope ratio analysis of N-containing organic compounds. *Rapid Commun. Mass Spectrom.* **2010**, *24*, 2849.
[33] F. Fourel, F. Martineau, C. Lécuyer, H. J. Kupka, L. Lange, C. Ojeimi, M. Seed. ^{18}O/^{16}O ratio measurements of inorganic and organic materials by elemental analysis-pyrolysis-isotope ratio mass spectrometry continuous-flow techniques. *Rapid Commun. Mass Spectrom.* **2011**, *25*, 2691.
[34] T. Boschetti, P. Iacumin. Continuous flow δ^{18}O measurements: new approach to standardization, high temperature thermodynamics and sulfate analysis. *Rapid Commun. Mass Spectrom.* **2005**, *19*, 3007.
[35] R. L. Grob, E. F. Barry. *Modern Practice of Gas Chromatography*. fourth. John Wiley & Sons, Inc.: Hoboken, New Jersey, **2004**.
[36] J. Savarino, B. Alexander, V. Darmohusodo, M. H. Thiemens. Sulfur and oxygen isotope analysis of sulfate at micromole levels using a pyrolysis technique in a continuous flow system. *Anal. Chem.* **2001**, *73*, 4457.
[37] U. Tsunogai, F. Nakagawa, D. D. Komatsu, T. Gamo. Stable carbon and oxygen isotopic analysis of atmospheric carbon monoxide using continuous-flow isotope ratio MS by isotope ratio monitoring of CO. *Anal. Chem.* **2002**, *74*, 5695.
[38] C. Spätl, T. W. Vennemann. Continuous-flow isotope ratio mass spectrometric analysis of carbonate minerals. *Rapid Commun. Mass Spectrom.* **2003**, *17*, 1004.
[39] W. M. Hagopian, A. H. Jahren. Minimization of sample requirement for δ^{18}O in benzoic acid. *Rapid Commun. Mass Spectrom.* **2010**, *24*, 2542.
[40] A. Kornfeld, T. W. Horton, D. Yakir, M. H. Turnbull. Correcting for nonlinearity effects of continuous flow isotope ratio mass spectrometry across a wide dynamic range. *Rapid Commun. Mass Spectrom.* **2012**, *26*, 460.
[41] T. Takaishi, A. Endoh. Exchange of oxygen isotopes between carbon dioxide and ion-exchanged zeolites. *A. J. Chem. Soc., Faraday Trans.* **1987**, *83*, 411.
[42] N. Mizuno, H. Mori, K. Mineo, M. Iwamoto. Isotopic exchange of oxygen between proton-exchanged zeolites and water. *J. Phys. Chem. B* **1999**, *103*, 10393.
[43] A. Faiia, X. Feng. Kinetics and mechanism of oxygen isotope exchange between analcime and water vapor and assessment of isotopic preservation of analcime in geological formations. *Geochim. Cosmochim. Acta* **2000**, *64*, 3181.
[44] O. Abe. Isotope fractionation of molecular oxygen during adsorption/desorption by molecular sieve zeolite. *Rapid Commun. Mass Spectrom.* **2008**, *22*, 2510.
[45] I. Ahn, M. Kusakabe, J. I. Lee. Oxygen isotopic fractionation of O_2 during adsorption and desorption processes using molecular sieve at low temperatures. *Rapid Commun. Mass Spectrom.* **2014**, *28*, 1321.

Supporting information

Additional supporting information may be found in the online version of this article at the publisher's website.